# Anatomic Variation of Depth-Dependent Mechanical Properties in Neonatal Bovine Articular Cartilage

**Jesse L. Silverberg,[1] Sam Dillavou,[1] Lawrence Bonassar,[2] Itai Cohen[1]**

[1]Department of Physics, Cornell University, C10 Clark Hall, Ithaca, New York 14853-2501, [2]Biomedical Engineering, Mechanical and Aerospace Engineering, Cornell University, Cornell University, Ithaca, New York

*Received 14 August 2012; accepted 4 December 2012*
*Published online 31 December 2012 in Wiley Online Library (wileyonlinelibrary.com). DOI 10.1002/jor.22303*

**ABSTRACT:** Articular cartilage has well known depth-dependent structure and has recently been shown to have similarly non-uniform depth-dependent mechanical properties. Here, we study anatomic variation of the depth-dependent shear modulus and energy dissipation rate in neonatal bovine knees. The regions we specifically focus on are the patellofemoral groove, trochlea, femoral condyle, and tibial plateau. In every sample, we find a highly compliant region within the first 500 μm of tissue measured from the articular surface, where the local shear modulus is reduced by up to two orders of magnitude. Comparing measurements taken from different anatomic sites, we find statistically significant differences localized within the first 50 μm. Histological images reveal these anatomic variations are associated with differences in collagen density and fiber organization.  J Orthop Res 31:686–691, 2013

**Keywords:** articular cartilage; depth-dependent mechanical properties; shear modulus; energy dissipation; biomechanics

Knowledge of normal synovial joint functioning, disease progression, and therapeutic treatments are strengthened by our understanding of articular cartilage (AC) mechanical properties. Because tissue engineered constructs do not yet fully mimic the biomechanical properties of native samples, the study of cartilage mechanics must stem from site-specific and cross-species studies performed with animal and human samples. Indeed, previous work has shown that within a single joint, anatomic variations exist in material properties such as compressive/aggregate modulus, permeability, Poison's ratio, and tissue thickness.[1–6] While many anatomic variation studies have employed compressive testing,[1–4] comparatively fewer have reported on shear properties,[5,6] resulting in a particularly acute knowledge gap, since shear loading is common during normal physiological conditions.

Studies quantifying AC shear properties generally report the equilibrium[7–11] or complex[12–18] shear modulus averaged over the tissue thickness. However, the collagen and proteoglycan networks underlying AC have well known depth-dependent heterogeneity.[19] Recent advances in rheometry techniques have made it possible to measure the depth-dependent shear modulus,[10,11,16–18] revealing localized variations analogous to those reported in the compressive properties of cartilage.[19–23] Notably, it was discovered that the superficial zone of neonatal bovine and adult human AC is 5–50 times more compliant under shear than the mechanically homogeneous mid and deep zones. These spatially localized variations in the mechanical properties are masked by bulk measurements, and their recent observation raises fundamental questions, such as how the depth-dependent shear properties, which parallel the depth-dependent structure of AC, vary with anatomic location.

The aim of this study was to measure and compare the depth-dependent shear modulus and energy dissipation rate of neonatal bovine AC harvested from the patellofemoral groove (PFG), trochlea (TRO), femoral condyles (FC), and tibial plateau (TP; Fig. 1). The PFG and TRO experience low in vivo loading, while the FC and TP experience high in vivo loading. Previous work suggests that tissue mechanical properties vary with loading conditions[1–6] and led us to hypothesize the existence of measureable differences in the shear properties. Moreover, the data gathered from all four regions provide useful biomechanical targets for tissue engineered constructs designed to mimic the properties of native tissue. Indeed, these results contribute to our still growing understanding in the depth-dependent shear properties in AC.

## METHODS

### Split-Line Test

We used split-line testing of the PFG, TRO, FC, and TP in 1–3 day old calf knees (Gold Medal Packing, Rome, NY) to identify suitable sites for mechanical testing.[24] Tissue from each region was rinsed with Delbecco's modified phosphate buffered saline (PBS, Life Technologies, Grand Island, NY) before Higgins India Ink (Chartpak, Inc., Leeds, MA) was applied to the articular surface. A rectangular grid pattern of sites was selected and a cylindrical needle 10 mm long and 1 mm wide was then inserted into the cartilage. Excess ink was washed off with PBS leaving behind a pattern of split-lines that were either oriented or symmetric. Denoting the direction normal to the articular surface as the transverse axis, oriented splits were used to identify zones of transverse anisotropy, while symmetric splits identified

Additional supporting information may be found in the online version of this article.

Grant sponsor: NSF; Grant number: DMR-1056662;
Grant sponsor: National Institutes of Health; Grant number: R21 AR054867;
Grant sponsor: National Science Foundation Graduate Research Fellowship

*Correspondence to*: Jesse L. Silverberg (T: 607-255-8853; F: 607-255-6428, E-mail: JLS533@cornell.edu)

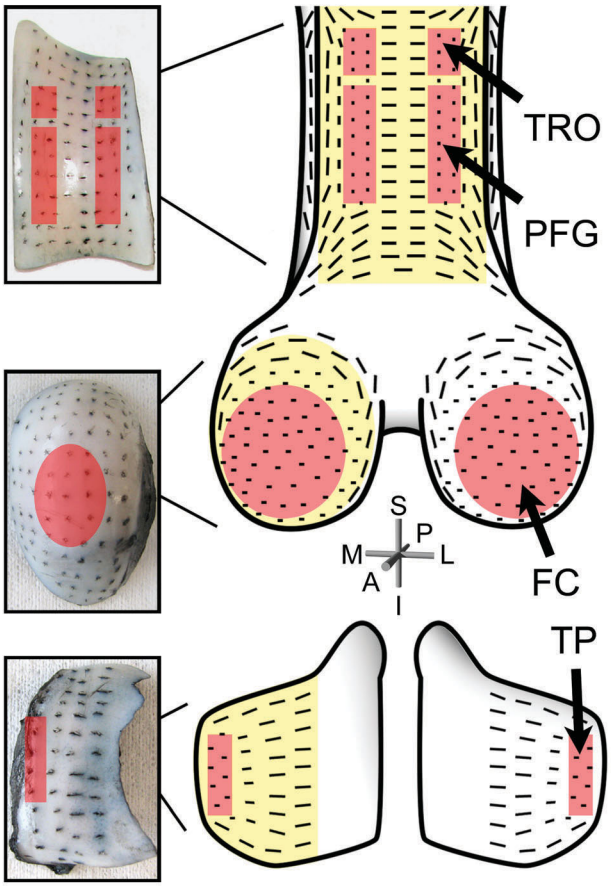


**Figure 1.** Split-line testing reveals the collagen fiber organization at the articular surface of neonatal bovine knee AC. Digital photographs (left) were taken and used to construct a schematic overview (right). Dots and lines indicate whether the tissue was isotropic or anisotropic, respectively. The zones highlighted in yellow correspond to the photographs and the zones in red are the sites where tissue for mechanical testing was harvested from.

zones of transverse isotropy. This test was repeated for two entire bovine knee joints and digital photographs were taken (Fig. 1). In zones of transverse isotropy, collagen fibers at the articular surface are randomly oriented in the articulating plane, yielding a material symmetry that causes the in-plane mechanical properties to be directionally independent.[25] Samples for shear testing were harvested from these zones to (1) preclude in-plane fiber orientation from introducing an uncontrolled source of sample-to-sample variation and (2) allow shear in any applied direction to deform AC tissue in a manner similar to shear applied in the direction of normal physiological loading.

### Materials

Cylindrical explants 3.5 mm thick and 6 mm in diameter were harvested with scalpel blades and biopsy punches from nine calf knees without the underlying bone tissue. They were then cut longitudinally into semi-cylinders and placed in a solution of PBS and 7 μg/ml 5-dichlorotriazinylamino-fluorescein (5-DTAF, Life Technologies), an all-protein stain, for 3 h. Afterwards, each sample was soaked in PBS for 1 h to rinse excess dye. A total of 13 samples from each anatomic region studied were mechanically tested within 24 h of harvesting.

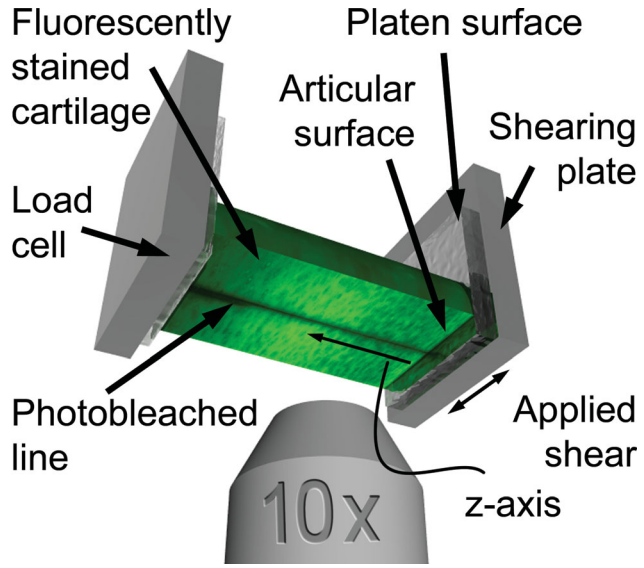


**Figure 2.** This schematic illustrates the basic geometry and operation of confocal strain mapping (see main text). Briefly, a line is photobleached onto the tissue to act as a fiducial marker and facilitate automated tracking of shear strain as a function of depth from the articular surface. Shear is applied by one plate, while load is simultaneously measured at the opposing side and deformations of the photobleached line are imaged with a fast confocal microscope.

### Confocal Strain Mapping

Fluorescently dyed semi-cylindrical cartilage samples were mounted in a Tissue Deformation Imaging Stage (TDIS, Harrick Scientific, Pleasantville, NY) so the long axis was perpendicular to the gripping surfaces,[17] allowing uniform shear forces to be applied on the articular surface (Fig. 2). To prevent slippage, samples were glued to a plate attached to a load cell, while friction between a platen plate and the articular surface was used to brace the opposing side where shear was applied. Friction was generated on the unglued surface by compressing samples by $8.0 \pm 0.5\%$ their initial thickness, and given 1 h to reach mechanical equilibrium. Once mounted, samples were immersed in PBS and the TDIS was positioned on an inverted Zeiss LSM 510 confocal microscope (Carl Zeiss, Germany) to image tissue deformations on the rectangular face of the semi-cylinder. Automated tracking of the local shear strain was facilitated by a photobleached line along the $z$ axis. We define $z$ to be the longitudinal direction, such that $z = 0$ is the articular surface and it measures depth into the tissue. Sinusoidal shear was applied at the physiologically relevant rate of 1.0 Hz (approximately walking speed) with a peak amplitude of 1% the compressed tissue thickness, consistent with the small strain approximation used in linear elasticity. Movies of tissue deformation recorded at 20 frames per second with a 10× objective were saved for later analysis.

Using Grid Resolution Automated Tissue Elastography[17] to analyze video data of the dynamic deformations, we calculated the complex shear modulus $G^*(z) = |G^*(z)| \exp(i\delta_\tau(z))$ as a function of depth $z$ (Fig. 3A–D). From our video data, we were also able to calculate the depth-dependent energy dissipation rate per unit volume.[18] For each sample, the total energy dissipated as a function of $z$ was normalized by the total energy dissipated per unit cycle (Fig. 3E–H). Comparisons of the modulus and energy dissipation among the four regions

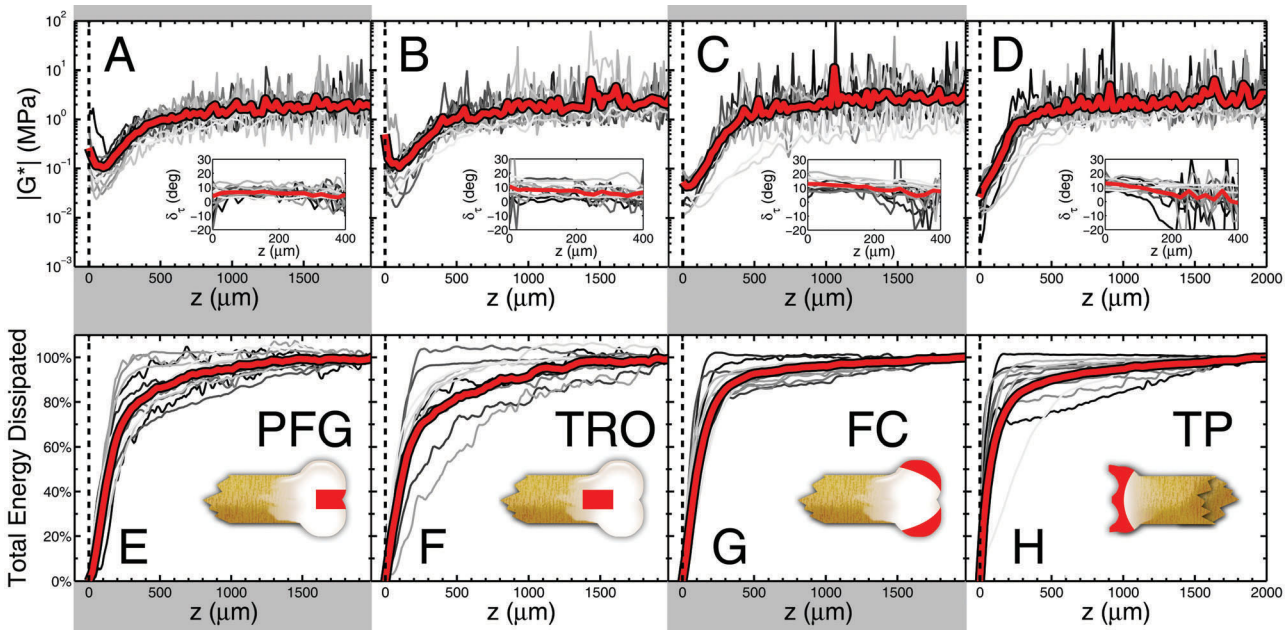


**Figure 3.** Measurements of the depth-dependent shear modulus $|G^*(z)|$ for the (A) PFG, (B) TRO, (C) FC, and (D) TP are plotted on a logarithmic axis as a function of depth. The articular surface is at $z = 0$, gray lines are individual measurements ($n = 13$ samples for each anatomic region), and the red lines are averages. We find the first 500 μm of tissue is 10–100 times more compliant than the remainder of the tissue. Insets show the phase angle $\delta_\tau$ of the complex shear modulus. Measurements of the cumulative energy dissipated as a function of depth for the (E) PFG, (F) TRO, (G) FC, and (H) TP show that the tissue near the articular surface is primarily responsible for viscous losses. Insets schematically illustrate the region from which tissue was harvested.

were performed along with tests for statistical significance (Fig. 4A–D).

### Brightfield and Polarized Light Histology

To image collagen content and organization, we fixed six samples from each anatomic region in 10% PBS-buffered formalin. Paraffinized sections 4 μm thick were dewaxed with xylene, rehydrated to water in decreasing concentration ethyl alcohol baths, and stained with Picrosirius red.[26,27] With a 40× objective, white and monochromatic light was used to observe collagen content, and white polarized light aligned parallel to the articuluar surface was used to determine fiber organization (Fig. 5A–D). All samples were stained simultaneously and viewed under identical lighting conditions.

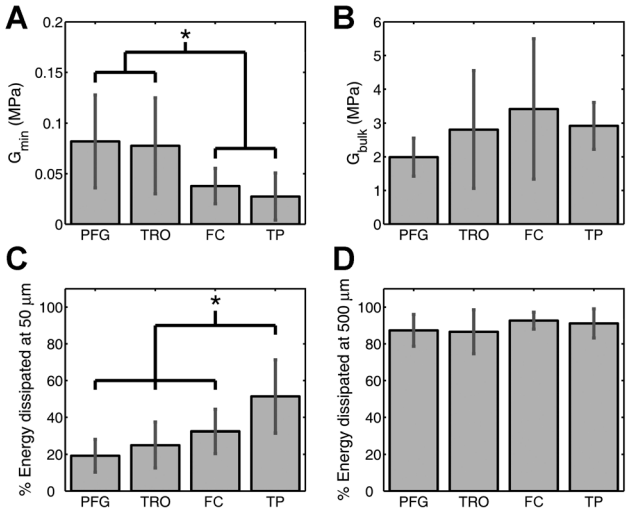


**Figure 4.** From our depth-dependent measurements, we compared (A) $G_{min}$, the minimum value of $|G^*(z)|$, (B) $G_{bulk}$, the average value of $|G^*(z)|$ for $z > 1{,}000$ μm, (C) the percent of energy dissipated within the first 50 μm of the articular surface, and (D) the percent of energy dissipated within the first 500 μm from the articular surface. In each case, averages and standard deviations are shown for the four anatomic regions studied ($n = 13$ for each anatomic region). Here, $^* = p < 0.05$, as determined from a balanced one-way ANOVA.

A semi-quantitative analysis was performed on monochromatic and polarized light histological images ($n = 6$ for each region) to facilitate comparisons of the depth-dependent pixel intensity between anatomic regions (Fig. 5A–D). For every sample, the tissue edge exhibited a slight roughness so that the articular surface had small fluctuations in position. To compensate, we used gradient edge detection techniques in MATLAB v7 (The Mathworks, Inc., Natick, MA) to identify the articular surface allowing us to uniquely define $z = 0$ for each column of pixels (see Supplementary Information). We then averaged columns of pixel intensity data within each image such that their $z$ position was properly registered, and normalized by the maximum possible pixel intensity value.

### Statistics

Data was analyzed with a balanced one-way ANOVA on each group and a post-hoc $t$-test using Tukey's honestly significant difference criterion to determine statistical significance ($p < 0.05$). All statistical analyses were carried out in MATLAB and expressed as a mean ± SD.

## RESULTS

Split-line testing in all four regions revealed transversely isotropic and anisotropic zones (Fig. 1). To ensure simple, consistent loading conditions, we used tissue from transversely isotropic zones with the flattest possible articular surface. For the PFG and TRO,

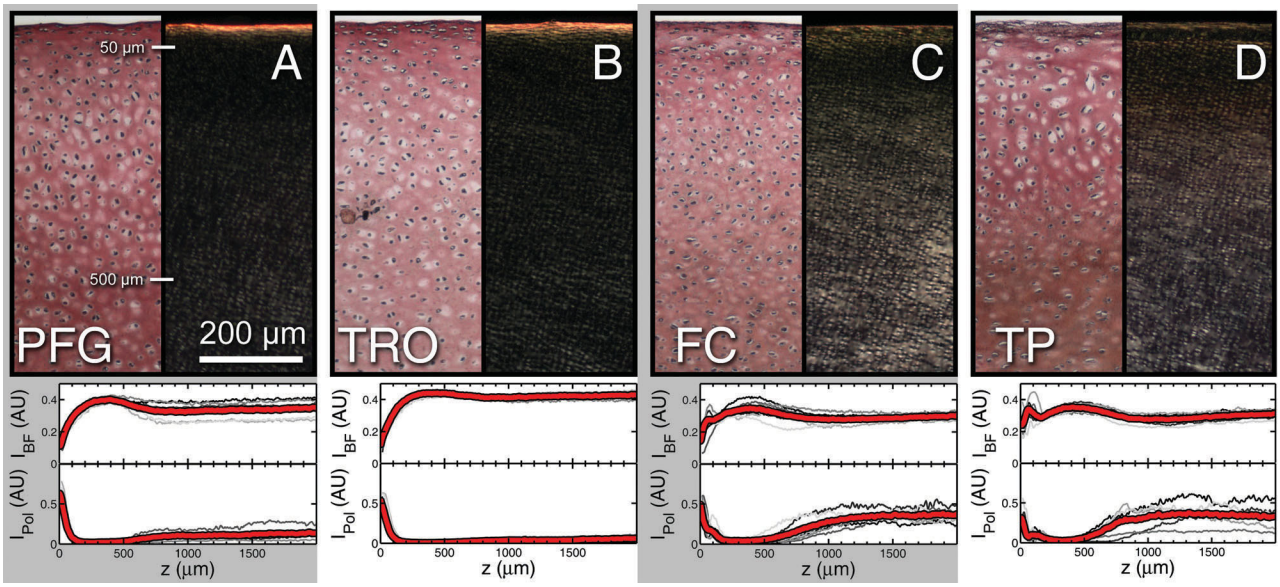


**Figure 5.** Cartilage sections were stained with Picrosirius red, then imaged with brightfield and polarized light under identical illumination conditions. Representative images shown here for the (A) PFG, (B) TRO, (C) FC, and (D) TP illustrate the similarities and differences between the four regions. To facilitate comparison between anatomic regions, we averaged the depth-dependent pixel intensity for brightfield monochromatic ($I_{BF}$) and polarized light ($I_{Pol}$), normalizing the data by the maximum possible intensity (arbitrary units). For each region, we plot these two semi-quantitative measures for individual images (gray) as well as the average (red; $n = 6$ for each anatomic region). All samples exhibit spatially localized depth-dependent variations of collagen density and fiber organization within the first 500 μm of tissue.

samples were harvested from a narrow region where the articular surface was nearly flat. For the FC, we found the tissue surface was rounded with a 2 ∼ 3 cm radius of curvature in the zone of transverse isotropy. Variations in surface height were <5%, and tissue harvested from this zone was chosen to minimize sample curvature. The TP has narrow zones of transverse isotropy in the most medial and lateral portions; though small in extent, at least two samples were reliably obtainable. These sites are covered by the meniscus in vivo, which we note is more compliant under compression than AC. Having identified transversely isotropic tissue from each anatomical region, we were able to harvest and mechanically test samples without tracking their in-plane orientation.

Our data show $|G^*(z)|$ varies with depth and location within the joint (Fig. 3A–D). Specifically, the average depth-dependent shear modulus for the FC is more compliant in the superficial zone than the PFG and TRO. Furthermore, the TP is the most compliant region tested, and within the measurement resolution, fails to exhibit the characteristic upswing in $|G^*(z)|$ near $z = 0$ seen in the other tested regions. For each sample, we extracted the minimum value of $|G^*(z)|$, hereafter referred to as $G_{min}$, and found that the FC and TP are more compliant than the PFG and TRO (Fig. 4A). We also calculated $G_{bulk}$, the average value of $|G^*(z)|$ for $z > 1{,}000$ μm, for each sample and found the four regions statistically indistinguishable (Fig. 4B).

Measurements of the complex phase angle $\delta_\tau$ revealed little depth-dependent variation in the PFG and TRO (Fig. 3A,B), while the FC and TP exhibited a slight but noticeable decline with increasing $z$ (Fig. 3C,D). Averaged over the first 400 μm of tissue, $\delta_\tau$ was $5 \pm 1^\circ$ for the PFG, $7 \pm 2^\circ$ for the TRO, $9 \pm 3^\circ$ for the FC, and $7 \pm 4^\circ$ for the TP. For $z > 400$ μm, the phase angle for all four regions was noisy, but tended to remain constant.

All four regions dissipate energy primarily near the articular surface, however, there is notable sample-to-sample variation: The least localized TP or FC can have a similar energy dissipation profile as the most localized PFG or TRO (Fig. 3E–H). To make quantitative comparisons, we measured the percent of energy dissipated within the first 50 and 500 μm of each sample. We found the TP has the greatest localization of energy dissipation (Fig. 4C), and all four regions dissipate indistinguishable amounts of energy by 500 μm (Fig. 4D).

Picrosirius red staining reveals depth-dependent variations similar to our rheological measurements. Brightfield and monochromatic images (Fig. 5A–D) show all four regions are more heavily stained where $z < 50$ μm relative to the tissue between 50 and 500 μm, indicating a highly localized collagen-dense band at the articular surface. Moreover, for $z > 500$ μm, we find minimal variation associated with depth. We also find that both the FC and TP exhibit localized bands of high collagen content near $z = 100$ μm not seen in the PFG or TRO.

Using polarized light, we see the PFG and TRO have a band of high birefringence where $z < 50$ μm and a 10-fold intensity reduction where $z > 50$ μm

(Fig. 5A,B). The FC and TP have more subtly modulated depth-dependent properties (Fig. 5C,D), and in particular, we see a region of low birefringence where $50 < z < 500$ μm, and an overall increase everywhere else. Furthermore, the birefringence of the PFG, TRO, and FC is higher than the TP at the articular surface, whereas the PFG and TRO exhibit noticeably less birefringence than the FC and TP for $z > 500$ μm. As with brightfield imaging, we see negligible depth-dependent variations in all four anatomic sites for $z > 500$ μm.

## DISCUSSION

Studying the depth-dependent complex shear modulus and energy dissipation rate in neonatal bovine AC revealed spatially localized, statistically significant differences near the articular surface associated with anatomic location. While tissue near the articular surface was consistently the most compliant portion of each sample, anatomic sites experiencing high levels of in vivo loading (FC, TP) were significantly more compliant than sites with low levels of in vivo loading (PFG, TRO). Furthermore, the TP dissipates more energy closer to the articular surface than the PFG, TRO, or FC. These differences in biomechanical properties associated with anatomical site are independent of regional cartilage thickness and coincide with depth-dependent heterogeneity in the AC collagen network. In the absence of theoretical models accounting for local collagen structure, the experimental data suggests a role for both collagen content and fiber orientation in setting the depth-dependent shear modulus and energy dissipation rate, but with no clear indication of their individual contributions. Similarly, no clear feature accounts for the lack of upswing in the TP shear modulus data near the articular surface, and it may arise from a convolution of collagen fiber orientation and density. While our results indicate potential targets for the development of complex, layered, and realistic engineered tissue constructs for therapeutic implantation,[28,29] additional studies are needed to precisely relate microscopic structural information to macroscopic material parameters.

We find broad agreement when comparing this work to previous studies of sheared bovine AC. For example, using 18 month old bovine PFG, measurements of the complex shear modulus averaged over the entire sample thickness reported $|G^*| = 0.75$ MPa and $\delta_\tau = 11^\circ$ when sheared at 1.0 Hz with a 9% axial compression.[14] Consistent with this earlier work, our depth-averaged measurement is $<|G^*(z)|>_{\mathrm{PFG}} \approx 0.6$ MPa. Similarly, a pair of studies examining 2–8 year old bovine TP with no axial compression reported the equilibrium shear modulus[8] $G_{\mathrm{eq}} = 0.38$ MPa, and the complex modulus[13] $|G^*| = 0.8$ MPa with a phase angle $\delta_\tau = 9.3^\circ$ when sheared at 100 Hz. Despite differences in age, shear rate, and loading conditions, these values are again comparable to our measurements. Finally, a study using the confocal strain mapping technique employed here sheared neonatal bovine PFG at 0.1 Hz and reported similar results for $|G^*(z)|$.[17]

While our results concern neonatal bovine tissue, quantitatively similar data have been reported in healthy adult human AC. Given differences in tissue age and thickness, this surprising result can be rationalized by noting that tissue maturity causes calcification and remodeling of the deep zone, and would not be expected to leave an age-dependent signature on the articular surface of healthy joints. For example, a pair of studies on human FC and TP tissue sheared under 0 and 15% axial compression[10,16] found the shear modulus was significantly lower within the first 800 μm when compared to the rest of the tissue. Values for the shear modulus of FC samples were typically $G_{\mathrm{eq}} = 0.2$ MPa near the articular surface and 1–3 MPa in the deep zone. Likewise, the TP was 0.02–0.03 MPa near the surface whereas the deep zone was also 1–3 MPa. While these results quantitatively agree with our findings in bovine AC, they are unable to resolve spatial variations smaller than 100–250 μm. In another study of adult human TP using the high resolution confocal strain mapping technique employed here,[17] spatial variations in $|G^*(z)|$ were observed at length scales approaching 10–15 μm. Specifically, highly localized variations near the articular surface similar to those observed in bovine PFG, TRO, and FC were reported. In order to determine whether this upswing in modulus at the articular surface is a general feature of human AC, a more detailed study controlling for split-line orientation, anatomic location, and tissue degradation due to age or disease would be necessary.

Because the depth-dependent shear properties of human tissue are quantitatively similar to bovine, the anatomic variations reported here may have relevance for tissue transfer procedures such as OATS® (Osteochondral Allo/Autograft Transfer System). In these therapeutic surgeries, AC focal injuries are repaired by replacing damaged tissue with tissue harvested from a cadaveric source or an unloaded region of the joint.[30,31] Because long-term success of these therapies depends on matching mechanical properties between donor and graft sites,[32] the measurements presented here raise the possibility of a previously unrecognized depth-dependent matching criterion for tissue selection. Although an analogous study with human tissue should be performed first, the ability to quantitatively match depth-dependent shear properties of donor and recipient tissue may be relevant for long-term patient outcomes.

We note some of the limitations of this study. To obtain large numbers of pristine joints, we used young tissue, potentially obscuring effects that may be important in adult animals such as disease and age-dependent remodeling of the collagen network.[33] Indeed, our work leaves unanswered whether these phenomena are accompanied by changes in the depth-dependent mechanical properties. Additionally, the experimental protocol used here to measure the shear modulus

takes advantage of the transverse isotropy identified in the split-line tests. For transversely anisotropic tissue, the protocol would have to be modified to track the primary split-line orientation throughout testing.

These results on the depth-dependent shear properties of bovine AC complement the existing literature on bulk shear properties. We identified a localized decrease in shear modulus occurring at the articular surface that distinguishes this tissue from the mid and deep zones. By studying distinct anatomic sites with different in vivo loading conditions, we found that all anatomic variation and nearly 90% of the energy dissipation is confined to the superficial zone. This new experimental data should stimulate further work examining the relationship between microscopic structure and macroscopic function, as well as provide new insights on normal and diseased cartilage functioning.

## ACKNOWLEDGMENTS

J.L.S. would like to thank D. Griffin, K. Novakofski, D. Lachowsky, L. Bradley, and M. Buckley for their insights and assistance. J.L.S. acknowledges support from the National Science Foundation through a Graduate Research Fellowship.

## REFERENCES

1. Simon WH. 1970. Scale effects in animal joints. Arthritis Rheum 13:244–255.
2. Athanasiou KA, Rosenwasser MP, Buckwalter JA, et al. 1991. Interspecies comparisons of in situ intrinsic mechanical properties of distal femoral cartilage. J Orthop Res 9: 330–340.
3. Froimson MI, Ratcliffe A, Gardner TR, et al. 1997. Differences in patellofemoral joint cartilage material properties and their significance to the etiology of cartilage surface fibrillation. Osteoarthritis Cartilage 5:377–386.
4. Kurkijarvi JE, Nissi MJ, Kiviranta I, et al. 2004. Delayed Gadolinium-enhanced MRI of cartilage (dGEMRIC) and $T_2$ characteristics of human knee articular cartilage. Magn Reson Med 52:41–46.
5. Jurvelin JS, Arokoski JPA, Hunziker EB, et al. 2000. Topographical variation of the elastic properties of articular cartilage in the canine knee. J Biomech 33:669–675.
6. Korhonen RK, et al. 2002. Importance of the superficial tissue layer for the indentation stiffness of articular cartilage. Med Eng Phys 24:99–108.
7. Parsons JR, Black J. 1977. The viscoelastic shear behavior of normal rabbit articular cartilage. J Biomech 10:21–29.
8. Spirt AA, Mak AF, Wassell RP. 1989. Nonlinear viscoelastic properties of articular cartilage in shear. J Orthop Res 7: 43–49.
9. Setton LA, Mow VC, Howell DS. 1995. Mechanical behavior of articular cartilage in shear is altered by transection of the anterior cruciate ligament. J Orthop Res 13:473–482.
10. Wong BL, et al. 2008. Biomechanics of cartilage articulation. Arthritis Rheum 58:2065–2074.
11. Buckley MR, Gleghorn JP, Bonassar LJ, et al. 2008. Mapping the depth dependence of shear properties in articular cartilage. J Biomech 41:2430–2437.
12. Woo SL, et al. 1987. Perichondrial autograft for articular cartilage. Acta Orthop Scand 58:510–515.
13. Simon WH, Mak A, Spirt A. 1989. The effect of shear fatigue on bovine articular cartilage. J Orthop Res 8:86–93.
14. Zhu W, Mow VC, Koob TJ, et al. 1993. Viscoelastic shear properties of articular cartilage and the effects of glycosidase treatments. J Orthop Res 11:771–781.
15. Stading M, Langer R. 1999. Mechanical shear properties of cell-polymer cartilage constructs. Tissue Eng 5:241–250.
16. Wong BL, Sah RL. 2010. Mechanical asymmetry during articulation of tibial and femoral cartilages. J Biomech 43:1689–1695.
17. Buckley MR, Bergou AJ, Fouchard J, et al. 2010. High-resolution spatial mapping of shear properties in cartilage. J Biomech 43:796–800.
18. Buckley MR, Bonassar L, Cohen I. 2012. Localization of viscous behavior and shear energy dissipation in articular cartilage under dynamic shear loading. J Biomech Eng DOI: 10.1115/1.4007454.
19. Mow VC, Ratcliffe A, Poole AR. 1992. Cartilage and diarthrodial joints as paradigms for hierarchical materials and structures. Biomaterials 13:67–97.
20. Schinagl RM, Ting MK, Price JH, et al. 1996. Video microscopy to quantitate the inhomogeneous equilibrium strain within articular cartilage during confined compression. Ann Biomed Eng 24:500–512.
21. Schinagl RM, Gurskins D, Chen AC, et al. 1997. Depth-dependent confined compression modulus of full-thickness bovine articular cartilage. J Orthop Res 15:499–506.
22. Chahine NO, Wang CC, Hung CT, et al. 2004. Anisotropic strain-dependent material properties of bovine articular cartilage in the transitional range from tension to compression. J Biomech 37:1251–1261.
23. Lai JH, Levenston ME. 2010. Meniscus and cartilage exhibit distinct intra-tissue strain distributions under unconfined compression. Osteoarthritis Cartilage 18:1291–1299.
24. Below S, Arzonczky SP, Dodds J, et al. 2002. The split-line pattern of the distal femur. Arthroscopy 18:613–617.
25. Cowin S, Doty S. 2007. Tissue mechanics, 1st ed. New York: Springer Science.
26. Rieppo J, et al. 2008. Practical considerations in the use of polarized light microscopy in the analysis of the collagen network in articular cartilage. Microsc Res Tech 71:279–287.
27. Junqueira LCU, Bignolas G, Brentani RR. 1979. Picrosirius staining plus polarization microscopy, a specific method for collagen detection in tissue sections. Histochem J 11:447–455.
28. Hung CT, et al. 2003. Anatomically shaped osteochondral constructs for articular cartilage repair. J Biomech 36:1853–1864.
29. Hung CT, et al. 2004. A paradigm for functional tissue engineering of articular cartilage via applied physiologic deformational loading. Ann Biomed Eng 32:35–49.
30. Lane JG, et al. 2001. A morphologic, biochemical, and biomechanical assessment of short-term effects of osteochondral autograft plug transfer in an animal model. Arthroscopy 17:856–863.
31. Mithoefer K, Hambly K, Villa SD, et al. 2009. Return to sports participation after articular cartilage repair in the knee. Am J Sports Med 37:167–176.
32. Ranawat AS, et al. 2008. Material properties of fresh cold-stored allografts for osteochondral defects at 1 year. Clin Orthop Relat Res 466:1826–1836.
33. Turnhout MvT, et al. 2010. Postnatal development of collagen structure in ovine articular cartilage. BMC Dev Biol 10: 1–16.